The Journal of Chemical Physics ARTICLE pubs.aip.org/aip/jcp

Catalyst-free activation and conversion of up to seven CO_2 by a B_6^+ monocation

Cite as: J. Chem. Phys. 164, 104301 (2026); doi: 10.1063/5.0321139
Submitted: 5 January 2026 • Accepted: 21 February 2026 •
Published Online: 9 March 2026

Qiang Chen,[1,a)] Rui-Nan Yuan,[1,2] Qin-Wei Zhang,[1] Hong Niu,[1] Rui Wei,[1] Zhi-Hong Wei,[1] Hai-Gang Lu,[1] Sheng-Gui He,[3,a)] and Si-Dian Li[1,a)]

AFFILIATIONS

[1] Institute of Molecular Science, Shanxi University, Taiyuan 030006, China
[2] Department of Materials Science and Chemical Engineering, Taiyuan University, Taiyuan 030000, China
[3] State Key Laboratory for Structural Chemistry of Unstable and Stable Species, Institute of Chemistry, Chinese Academy of Sciences, Beijing 100190, China

[a)] **Authors to whom correspondence should be addressed:** chenqiang@sxu.edu.cn; shengguihe@iccas.ac.cn; and lisidian@sxu.edu.cn

ABSTRACT

Exploring advanced materials for efficient activation and conversion of CO_2 is a crucial approach to mitigate climate change and reduce reliance on fossil fuels. Extensive joint gas-phase mass spectroscopy and kinetic studies performed herein indicate that a mass-selected B_6^+ monocation can consecutively activate and convert up to seven CO_2 to CO under ambient conditions, setting up a record number of CO_2 molecules that an isolated cluster can activate in experiments. Detailed theoretical calculations and analyses reveal the ground-state, intermediate, and transition-state geometries as well as CO_2-activation and CO-desorption pathways of the concerned species. The catalyst-free CO_2-reduction reactions $B_6^+ + nCO_2 \rightarrow B_6O_n^+ + nCO$ (n = 1–7) all appear to be barrier-free in kinetics and thermodynamically favorable at room temperatures, with the calculated exothermicities increasing almost linearly with the number (n) of CO_2 molecules activated in the processes. Two electron-deficient periphery B atoms in $B_6O_n^+$ (n = 0–6) are found to serve as active sites to form one effective σ-donation and two weak π-back-donations each in two consecutive steps, with the first site activating a π-bond in O=C=O to form the O≡C–O-adsorption states, while the second site releasing a CO molecule from the CO-desorption states to form the final products, $B_6O_n^+$, unveiling the important role of boron as a honorary transition metal in CO_2 activation and conversion.

I. INTRODUCTION

With increasing awareness of green chemistry and sustainable development, direct conversion of abundant and cheap CO_2 into useful chemicals can effectively help reduce greenhouse gas emissions and obtain high value-added chemicals.[1–4] However, the high thermodynamic stability and kinetic inertness of CO_2 in its chemical transformation make the activation and utilization of CO_2 extremely challenging.[5] CO_2 has been utilized mainly through its reductions, including catalytic hydrogenation,[2] electrochemistry,[6] thermal catalysis, photocatalysis,[7] and photoelectric synergistic catalysis[8] to obtain methanol, formic acid, dimethyl ether, and other products. However, these technologies usually require unique metal catalysts or high energy (such as light, electricity, or thermal energy) to induce the reactions or have low utilization efficiency and poor selectivity. Metal-based materials are the best-known catalysts in the activation of CO_2.[9–11]

Boron (B[Ar]$2s^2 2p^1$) as a prototypical electron-deficient element is known to exhibit metallomimetic properties.[12–16] Persistent joint photoelectron spectroscopy and first-principles theory investigations over the past two decades have shown that boron cluster monoanions (B_n^-) favor planar or quasi-planar structures for at least up to B_{42}^-,[17–20] with cage-like B_{40}^- and B_{28}^- minor isomers and ground-state cage-like B_{39}^-,[21–23] bilayer B_{48}^-,[24] core–shell B_{46}^- (B_2@B_{44}^-), and nest-like B_{56}^- (B_{12}@B_{44}^-)[25] observed consecutively in experiments. For cationic boron clusters (B_n^+), double-ring tubular structures are confirmed between n = 16–25 in ion-mobility experiments.[26] In 2015, Braunschweig and co-workers synthesized a stable borylene dicarbonyl complex in the condensed phase.[12]

More recently, boron has been observed to exhibit transition-metal-like behaviors in a series of gas-phase clusters, including its boronyl (BO) monoanion (B_9O^-),[13] and carbonyl (CO) complexes: $B_{13}(CO)_n^+$,[14] $B_{11}(CO)_n^+/B_{15}(CO)_n^+$,[15] and $B_{20}(CO)_n^+$.[16] In condensed-phase studies, boron-containing compounds have been found to promote the conversion of small molecules, such as CH_4, CO_2, N_2, and CO.[27–33] In 1991, Ruatta *et al.* observed the dominant CO_2-reduction reactions of $B_m^+ + CO_2 \rightarrow B_mO^+ + CO$ (m = 1–14) in gas-phase experiments, but with no consecutive reactions of B_m^+ with multiple CO_2 molecules explored.[34] Chen *et al.* found in 2018 that gas-phase CuB^+ cluster can couple CH_4 with CO_2 under thermal collision conditions to produce ketene ($H_2C{=}C{=}O$).[35] Subsequently, Ma and colleagues reported that the $Nb_2BN_2^-$ anion could continuously convert up to four CO_2 molecules to CO and found that B atom plays a crucial role in the activating and converting processes.[36] They reported the first metal-free $B_2O_2^-$ late that could continuously activate up to two CO_2.[37] Recently, they discovered that $Nb_3C_4^-$ can continuously convert five CO_2 to CO, presenting a metal–non-metal binary cluster that can activate and convert the maximum number of CO_2 molecules reported to date.[38] In 2023, He *et al.* discovered that Co_{12}^- and Co_{13}^- metal cluster monoanions could also consecutively activate up to five CO_2 molecules.[39] Chen *et al.* found in 2025 that B_{56}^- monoanion was able to chemisorb and activate one CO_2 molecule, even partially releasing CO to produce $B_{56}O^-$.[25] However, the consecutive activation and conversion of multiple CO_2 molecules by a size-selected more electron-deficient B_m^+ monocation still remain elusive to date in literature.

In this work, we report the catalyst-free activation and conversion of up to seven CO_2 molecules to CO by a B_6^+ monocation under ambient conditions, as revealed by joint time-of-flight mass spectroscopy and first-principles theory investigations, setting up a record number of CO_2 molecules activated by a bared nanocluster in gas phase. Detailed theoretical calculations and analyses unveil the kinetic mechanisms for the $B_6^+ + nCO_2 \rightarrow B_6O_n^+ + nCO$ CO_2-reduction reactions (n = 1–7). Two electron-deficient periphery B atoms in $B_6O_n^+$ monocations (n = 0–6) are found to serve as active sites in two consecutive steps to form one effective σ-donation and two weak π-back-donations each with the O=C=O and C≡O σ-ligands, indicating that boron exhibits transition-metal-like behaviors in CO_2 activation and conversion.

II. METHODS

A. Experimental methods

Using a home-made reflection time-of-flight mass spectrometer (TOF-MS) equipped with a laser ablation cluster source, a quadrupole mass filter (QMF),[40] and a linear ion trap reactor (LIT),[41] we studied the reactions of mass-selected B_m^+ (m = 5–15) with CO_2 in gas-phase experiments. The bare boron clusters B_m^+ (m = 5–15) were generated by laser ablation of a rotating and translating ^{11}B isotope target (99% enriched) in the presence of a 2 atm He carrier gas. A 532 nm (second harmonic of Nd_3^+: yttrium aluminum garnet-YAG) laser with an energy of 3–5 mJ/pulse and a repetition rate of 10 Hz was used. The B_m^+ (m = 5–15) cluster cations were mass-selected by the QMF and entered into the LIT reactor, where they were confined and thermalized by collisions with a pulse of He gas for 2 ms and cooled to room temperature and then interacted with a pulse of reactant gas ($C^{16}O_2$ or $C^{18}O_2$) for different reaction times. The cluster monocations ejected from the LIT reactor were detected by the TOF-MS.[42]

The pseudo-first-order rate constants (k_1) of the reactions between the B_6^+ cluster and CO_2 were determined using the following equation:

$$\ln \frac{I_R}{I_T} = -k_1 \frac{P}{k_B T} t_R, \quad (1)$$

in which I_R is the intensity of the reactant cluster ions after the reaction, I_T is the total ion intensity including product ion contribution, T is the temperature (~300 K), P is the effective pressure of the reactant gas in the ion trap reactor, t_R is the reaction time, and k_B is the Boltzmann constant. More details about the method used to derive k_1 can be found in Ref. 43.

B. Theoretical methods

Density functional theory (DFT) calculations were carried out to optimize the structures of reactant B_6^+ and products $B_6O_n^+$ (n = 1–7) as well as the reaction pathways of $B_6O_n^+$ (n = 0–7) monocations with CO_2 at the B3LYP level,[44–46] with the aug-cc-pvtz (AVTZ) basis set used for B, C, and O.[47,48] The widely used B3LYP hybridized density functional has proven to be reliable for small bared boron clusters.[17] To verify the ground-state structure of B_6^+ (**iso 1**, C_{2h} ^2B_u), the relative energies of the first four lowest-lying isomers of B_6^+ were further refined by employing single-point calculations at CCSD(T)/AVTZ//B3LYP/AVTZ[49–51] and CASPT2(7,8)//CASSCF(7, 8)/AVTZ[52,53] (complete active-space second-order perturbation theory with the AVTZ basis set, with seven electrons and eight orbitals forming the active space). Global searches for the most stable structures of the product ions $B_6O_n^+$ (n = 1–7) were performed using the TGMin2 program.[54,55] The reaction mechanism explorations involve the geometrical optimization of both the intermediates (IMs) and transition states (TSs). Vibrational frequency analyses were performed to ensure the IMs and TSs have zero and only one imaginary frequency, respectively. The intrinsic reaction coordinate (IRC) calculations were carried out to make sure that each TS connects two appropriate minima.[56,57] More accurate relative energies for all species along the reaction pathways of $B_6^+ + nCO_2$ (n = 1–7) were obtained from single-point CCSD(T)/AVTZ calculations based on B3LYP/AVTZ optimized geometries. The zero-point-correction-included energies (ΔE_0) in the unit of eV were reported in this work.

All DFT and CCSD(T) calculations were carried out using the Gaussian 16 program,[58] while CASPT2 calculations were performed using the MolPro 2012.1 package.[59] Natural bond orbital (NBO) analyses were performed using NBO 6.0.[60] Born–Oppenheimer molecular dynamics (BOMD) simulations were performed on product ions $B_6O_n^+$ (n = 1–7) for 100 ps with the GTH-PBE0 pseudopotentials and TZVP-MOLOPTPBE-GTH basis sets[61,62] using the CP2K software package suite.[63] Detailed bonding analyses were performed using the widely used adaptive natural density partitioning (AdNDP) method.[64] Energy decomposition analyses with natural orbitals for chemical valence (EDA-NOCV)[65–67] were performed to analyze the coordination interactions in the concerned CO_2-adsorption and CO-desorption states at the PBE0/TZ2P level using the ADF 2022 program package.[68]

III. RESULTS

A. Experimental results

The size-selected bare boron clusters B_m^+ (m = 5–15) were confined and cooled at room temperature and then reacted with CO_2 in the LIT reactor under thermal collision conditions.

As shown in Fig. S1, the intensity of B_6^+ is most significantly reduced by a 4.9 mPa CO_2 reactant gas in the size range between B_5^+–B_{17}^+, followed by B_5^+. We, therefore, choose B_6^+ as a prototypical example to explore the reaction mechanisms of B_m^+ monocations with CO_2. The TOF mass spectra in Fig. 1(A) show the reactions of mass-selected B_6^+ with $C^{16}O_2$ at various pressures, with the corresponding kinetic studies illustrated in Fig. 1(B). Figure 1(A)(a1) shows the background spectrum of B_6^+ in collision with noble gas (He). Upon the reaction of B_6^+ with 0.8 mPa CO_2 [Fig. 1(A)(a2)], signal peaks for B_6O^+ and $B_6O_2^+$ appeared. The presence of B_6O^+ indicates that B_6^+ could reduce CO_2 to release CO. The appearance of a weak signal of $B_6O_2^+$ suggests that the product B_6O^+ can further react with a second CO_2. As the CO_2 partial pressure increases from 1.8 to 18.9 mPa [Fig. 1(A)(a3)–(a6)], a series of boron oxide clusters are clearly formed, from B_6O^+ to the oxygen-rich product $B_6O_7^+$. Isotope labeling experiments using the $C^{18}O_2$ reactant shown in Fig. S2 further confirm that B_6^+ can continuously convert seven CO_2 molecules into CO. The experimental mass spectra clearly show that a single B_6^+ monocation can successively activate and convert up to seven CO_2 molecules to CO in reaction (2),

$$B_6^+ + nCO_2 \rightarrow B_6O_n^+ + n\,CO \quad (n = 1\text{–}7). \tag{2}$$

In addition, when the CO_2 partial pressure was further increased to 87 mPa, weak product signals assigned to $B_6O_nCO_2^+$ (n = 4–7) were observed (Fig. S2), suggesting that $B_6O_n^+$ (n = 4–7) can also form CO_2 adsorption products at higher CO_2 pressures. The mass spectral data for the reactions of other mass-selected B_m^+ monocations (m = 5, 7–15) with CO_2 are illustrated in Figs. S3 and

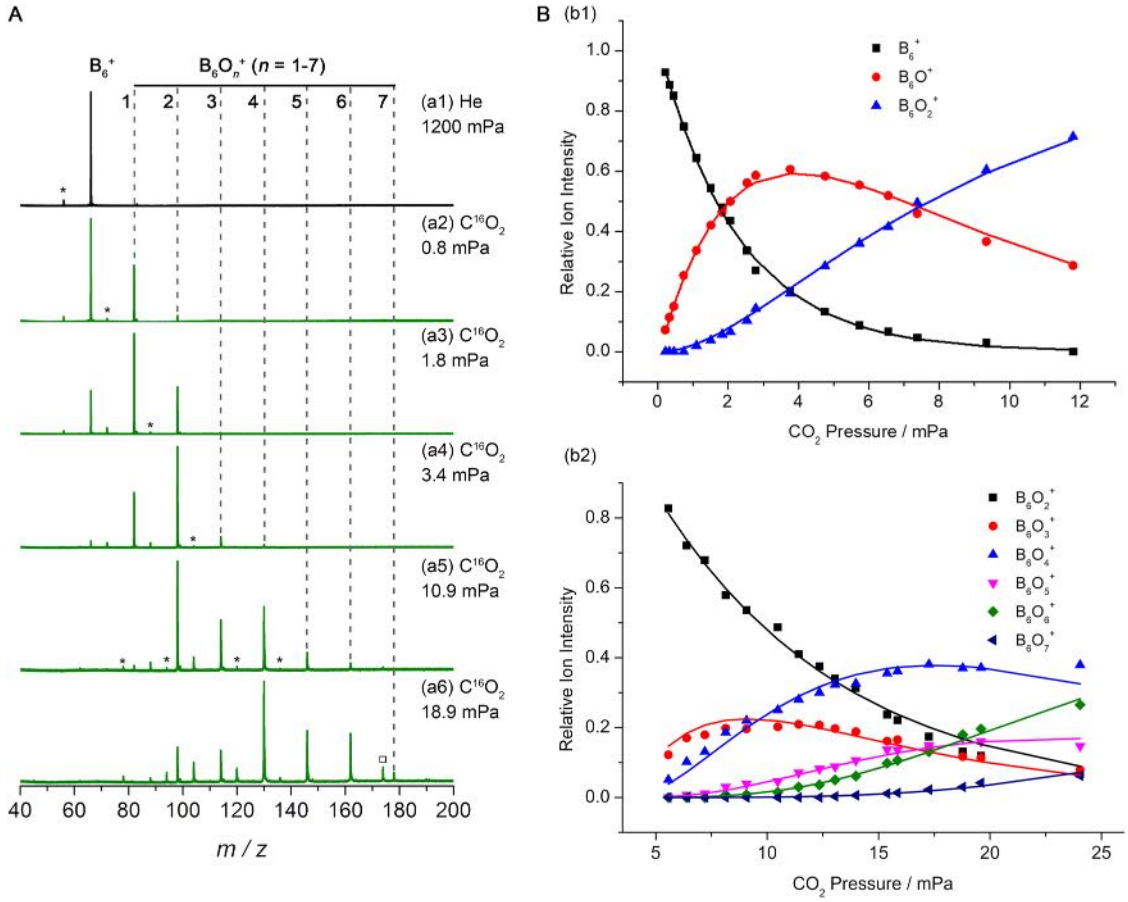

FIG. 1. (A) Time-of-flight (TOF) mass spectra for the reactions of mass-selected B_6^+ with He (a1) and $C^{16}O_2$ (a2)–(a6), with the pressures of reactant gas indicated. The reaction time is about 2.0 ms. The weak mass signals marked with asterisks are due to existence of water impurities in the reaction system. The peak marked with a hollow square in (a6) corresponds to the CO_2-absorption species of $B_6O_4CO_2^+$ ($B_6O_4^+ + CO_2 \rightarrow B_6O_4CO_2^+$). (B) Variation of relative intensities of reactant and product ions with respect to the reactant gas effective pressures in the reaction of B_6^+ with CO_2. The reaction times in panels (b1) and (b2) are 0.5 and 2.0 ms, respectively. The solid lines are fitted to experimental data points with the approximation of the pseudo-first-order reaction mechanism.

S4, wherein both B_5^+ and B_{11}^+ appear to be able to activate up to four CO_2 consecutively and B_7^+, B_8^+, B_9^+, B_{10}^+, B_{12}^+, B_{14}^+, and B_{15}^+ can activate one to three CO_2, while the experimentally known highly stable aromatic magic B_{13}^+ appears to be inert toward CO_2. It should be noticed that bigger B_m^+ clusters with $m \geq 10$ exhibit much lower reactivities toward CO_2 than B_6^+, with much higher CO_2 pressures and longer reaction times used in Figs. S3 and S4 than in Fig. 1.

Based on the least-square fitting procedure shown in Fig. 1(b), the pseudo-first-order rate constants of $B_6O_n^+ + CO_2 \rightarrow B_6O_{n+1}^+ + CO$ were estimated to be k_1 = 35.9, 11.1, 2.46, 5.83, 1.96, 3.88, and 0.78×10^{-10} cm^3 molecule^{-1} s^{-1} for n = 0, 1, 2, 3, 4, 5, and 6, respectively (Table I). B_6^+ appears to have the largest first rate constant k_1 toward CO_2 in available gas-phase clusters reported to date in the literature. For examples, the pseudo-first-order rate constants of V_2^+ and V_2O^+ with CO_2 were estimated to be $k_1 = 3.8 \times 10^{-12}$ and 8.8×10^{-10} cm^3 molecule^{-1} s^{-1},[69] respectively, that of $Nb_3C_4^-$ was $k_1 = 7.8 \times 10^{-10}$ cm^3 molecule^{-1} s^{-1},[38] and for both Co_{12}^- and Co_{13}^-, the rate constant was $k_1 = 1.5 \times 10^{-10}$ cm^3 molecule^{-1} s^{-1}.[39] The rate curves and corresponding first-order rate constants for the reactions of other boron cluster monocations B_m^+ (m = 5, 7–15) with CO_2 are shown in Figs. S5 and S6 and Table S1. B_6^+, which can react with up to seven CO_2 molecules consecutively, turns out to have the largest first-order rate constant of $k_1 = 3.59 \times 10^{-9}$ cm^3 molecule^{-1} s^{-1} in the B_m^+ series (m = 5–15), with B_5^+ being the second with $k_1 = 2.89 \times 10^{-9}$ cm^3 molecule^{-1} s^{-1}, consistent with the signal intensity distributions observed in Fig. S1.

TABLE I. Estimated pseudo-first-order rate constants (k_1) for the reactions of $B_6O_n^+ + CO_2 \rightarrow B_6O_{n+1}^+ + CO$ (n = 0–6) from the kinetic data obtained in Fig. 1(B) using Eq. (1).

Reactions	k_1 (cm^3 molecule^{-1} s^{-1})
$B_6^+ + CO_2 \rightarrow B_6O^+ + CO$	3.59×10^{-9}
$B_6O^+ + CO_2 \rightarrow B_6O_2^+ + CO$	1.11×10^{-9}
$B_6O_2^+ + CO_2 \rightarrow B_6O_3^+ + CO$	2.46×10^{-10}
$B_6O_3^+ + CO_2 \rightarrow B_6O_4^+ + CO$	5.83×10^{-10}
$B_6O_4^+ + CO_2 \rightarrow B_6O_5^+ + CO$	1.96×10^{-10}
$B_6O_5^+ + CO_2 \rightarrow B_6O_6^+ + CO$	3.88×10^{-10}
$B_6O_6^+ + CO_2 \rightarrow B_6O_7^+ + CO$	7.81×10^{-11}

B. Theoretical results

Extensive first-principles theory calculations have been performed to investigate the CO_2-activation and CO-desorption pathways of $B_6O_n^+$ (n = 0–7) monocations shown in Figs. 2 and S7–S18. As shown in Fig. 3, in the most favorable pathways, the $B_6^+ + nCO_2$

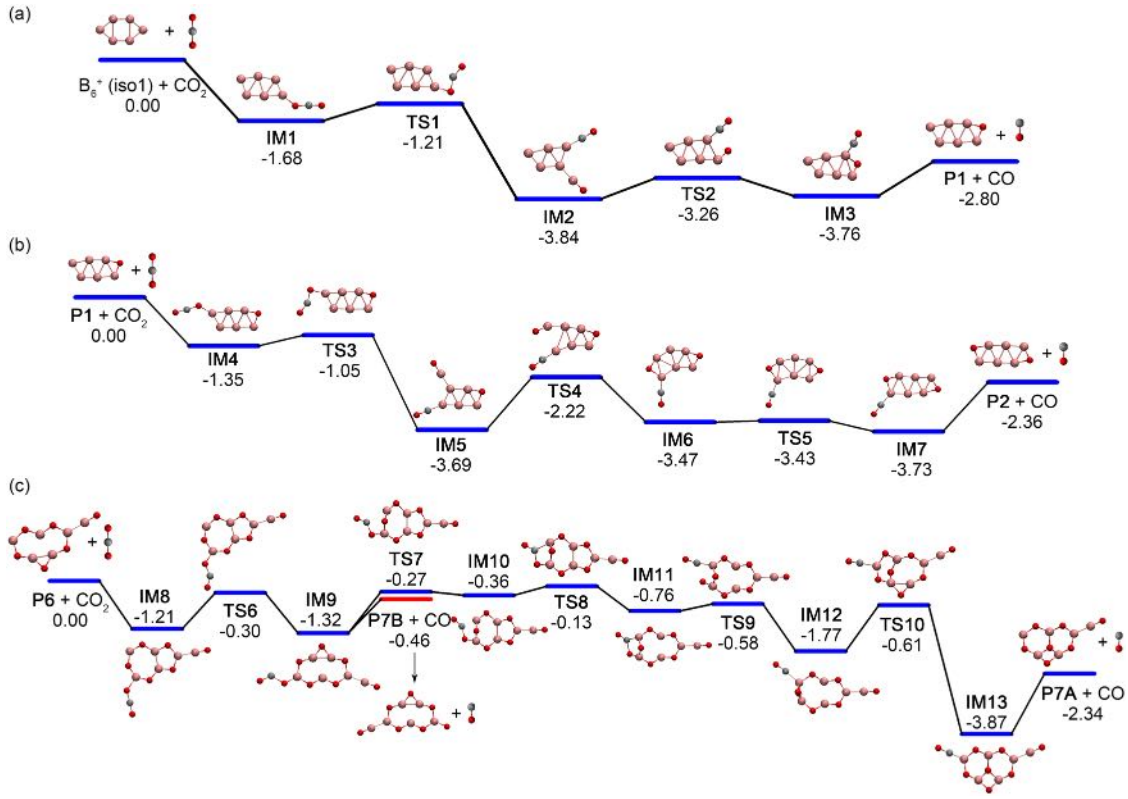

FIG. 2. CO_2-activation and CO-desorption pathways of (a) $B_6^+ + CO_2 \rightarrow B_6O^+ + CO$, (b) $B_6O^+ + CO_2 \rightarrow B_6O_2^+ + CO$, and (c) $B_6O_6^+ + CO_2 \rightarrow B_6O_7^+ + CO$, with the relative energies indicated in eV at CCSD(T).

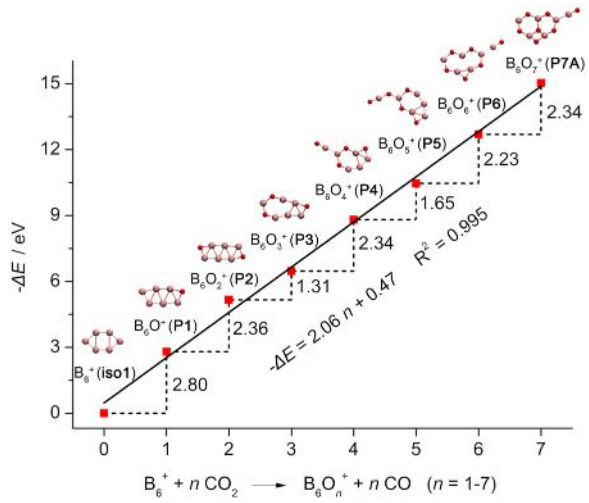

FIG. 3. Optimized global minimum structures of the $B_6O_n^+$ (n = 1–7) boron oxide cluster monocations and variation of their calculated exothermicities ΔE = (E_{B6On+} + nE_{CO}) − (E_{B6+} + nE_{CO2}) with respect to reactions of B_6^+ + nCO_2 → $B_6O_n^+$ + nCO (n = 1–7) at CCSD(T).

→ $B_6O_n^+$ + nCO reactions (n = 1–7) all appear to be highly exothermic, with the calculated exothermicities increasing almost linearly with the number (n) of CO_2 molecules involved in the processes: $\Delta E = -2.06n - 0.47$. The reactions possess the overall calculated exothermicity of ΔE = −15.03 eV from n = 1 to 7 and an average exothermicity of 2.06 eV per CO_2. Extensive BOMD simulations were performed on the most stable $B_6O_n^+$ (n = 1–7) isomers to examine their dynamic stabilities. As clearly shown in Fig. S19, these boron oxide products all appear to be highly dynamically stable at 500 K in 100 ps, with the small calculated root-mean-square deviations of RMSD = 0.05–0.06 Å and maximum bond length deviations of MAXD = 0.11–0.16 Å, respectively.

As the size of boron oxide clusters increases, the first boronyl group (–BO) occurs in $B_6O_4^+$ (**P4**), the first highly stable BO_3 triangular structural unit observed in B_3O_2 crystal emerges in $B_6O_5^+$ (**P5**), while the first two neighboring B_3O_3 hexagons existing in solid B_2O_3 appear in $B_6O_7^+$ (**P7**) (Fig. 3). Oxygen atoms in most cases serve as bridges between two neighboring B atoms, except in –BO terminals. Alternative low-lying isomers of $B_6O_n^+$ (n = 0–7) are depicted in Figs. S7–S9. As shown in Figs. S10 and S11, the relaxed potential energy curves indicate that the approaches of CO_2 to $B_6O_n^+$ monocations (n = 0–6) and formations of stable adsorption complexes $B_6O_n(CO_2)^+$ are overall barrier-free processes. As demonstrations, Fig. 2 shows the specific CO_2-reduction pathways for the reactions of (a) B_6^+ + CO_2 → B_6O^+ + CO, (b) B_6O^+ + CO_2 → $B_6O_2^+$ + CO, and (c) $B_6O_6^+$ + CO_2 → $B_6O_7^+$, respectively, with the intermediate states (IMs), transition states (TSs), and final products (Ps) depicted and their relative energies with respect to the entrance channel indicated at CCSD(T). Detailed potential energy profiles for the remaining $B_6O_n^+$ species (n = 0–7) are presented in Figs. S12–S18.

The low-lying isomers of B_6^+ were reexamined at the CCSD(T) and CASPT2 levels. CCSD(T)/AVTZ calculations turned out to have high T1 diagnosis factors (T1 > 0.05) for **iso 1** and **iso 2**, indicating that multi-reference interactions cannot be neglected in B_6^+ monocation. At the CASPT2(7,8)//CASSCF(7,8)/AVTZ level, the previously proposed low-lying D_{2h} B_6^+ (**iso 2,** $^2B_{1u}$), C_s B_6^+ (**iso 3,** $^2A'$), and C_{2h} B_6^+ (**iso 4,** ^2B_g)[17,70–72] isomers are found to be 0.02, 0.03, and 0.65 eV less stable in energy than C_{2h} B_6^+ (**iso 1,** ^2B_u), respectively (Fig. S7). The perfectly planar C_{2h} B_6^+ (**iso 1,** ^2B_u) is, therefore, identified as the global minimum of B_6^+ at CASPT2(7,8), which possesses two equivalent di-coordinate vertex B atoms with the largest calculated net natural atomic charge of +0.407|e| (Fig. S20). Intriguingly, as shown in Figs. 2(a), S10, and S12, the CO_2-reduction pathways of these four B_6^+ isomers all appear to be barrier-free kinetically, and more importantly, they all ultimately lead to the same thermodynamically most stable product of C_s B_6O^+ (**P1**), in agreement with the experimental observation that B_6^+ exhibits no inert isomers in Fig. 1(A). Figure 2(a) indicates that in the CO_2-adsorption state $[B_6–O–C{\equiv}O]^+$ (**IM1**), which has the adsorption energy of ΔE = 1.68 eV at CCSD(T), the first :O=C=O: σ-ligand is barrierlessly coordinated to one of the two di-coordinate vertex B atoms in C_{2h} B_6^+ (**iso 1**) (Fig. S20). **IM1** can be transferred barrierlessly to the most stable intermediate state $[OB–B_5–CO]^+$ (**IM2**), which contains a carbonyl ligand (–CO) coordinated to the second active di-coordinate B atom and a boronyl group (–BO) coordinated to a tri-coordiante periphery B atom via the transition state **TS1** with the negative barrier of −1.21 eV. The –BO boronyl group in **IM2** is transformed to the CO-desorption state $[OB_6–CO]^+$ (**IM3**), which contains a bridging O atom between the two active sites via **TS2** with the negative barrier of −3.26 eV. **IM3** releases its CO ligand to form the final product of C_s B_6O^+ (**P1**) observed in Fig. 1(A)(a1) with the overall exothermicity of 2.80 eV. Detailed reduction mechanisms of the second, third, and fourth isomers of B_6^+ (**iso 2, iso 3,** and **iso 4**) with CO_2 are collectively shown in Fig. S12. We address here that the reactions of all the four lowest-lying isomers of B_6^+ with CO_2 ultimately lead to the same thermodynamically most stable oxide B_6O^+ (**P1**), although in slightly different mechanisms.

As indicated in Fig. 2(b), in the CO_2-adsorption state of $[OB_6 \leftarrow O–C{\equiv}O]^+$ [**IM4**] with the adsorption energy of ΔE = 1.35 eV, the second :O=C=O: is coordinated to the most protruding di-coordinate periphery B atom in C_s B_6O^+ (**P1**) at the opposite end. **IM4** can be converted to **IM5**, which contains a –CO ligand coordinated to the second active di-coordinate B atom via **TS3** with the negative relative energy of −1.05 eV. **IM5** can be spontaneously converted to the final product of C_{2h} $B_6O_2^+$ (**P2**) with the overall exothermicity of ΔE = 2.36 eV via **TS4** and **TS5**, which both possess negative energy barriers, resulting in the strong mass peaks observed for $B_6O_2^+$ in both Fig. 1(A)(a3) and (a4). Another parallel but more complicated pathway in Fig. S13 may coexist in experiments, which has the same active sites and generates the same thermodynamically stable product **P2** as in Fig. 2(a), but is different in specific kinetic mechanisms. Similar but more complicated reaction pathways have also been obtained for $B_6O_2^+$, $B_6O_3^+$, $B_6O_4^+$, and $B_6O_5^+$, which can react with the third, fourth, fifth, and sixth CO_2 in barrier-free processes to produce $B_6O_3^+$, $B_6O_4^+$, $B_6O_5^+$, and $B_6O_6^+$ in Figs. S14–S17, respectively. As indicated in Fig. 2(c), the much concerned C_s $B_6O_6^+$ (**P6**) also possesses two periphery B atoms separated by a bridging O atom as two active sites to react with the seventh CO_2 in the most favorite pathway to produce the final product C_1 $B_6O_7^+$ (**P7A**) with the exothermicity of 2.34 eV. $B_6O_7^+$ (**P7A**) is the first

boron oxide cluster containing two neighboring B_3O_3 hexagons in the $B_6O_n^+$ series (n = 1–7). Although CO-dissociation from **IM9** → **P7B** + CO is kinetically favored over the internal conversion of **IM9** → **TS7**, the much higher thermodynamic stability of **P7A,** which is 1.88 eV lower in energy than **P7B** at CCSD(T), together with overall exothermicity (12.69 eV) of the preceding six-step reactions, may facilitate the formation of **P7A** in Fig. 2(c).

The Rice–Ramsperger–Kassel–Marcus (RRKM) theory and RRKM-based variational transition-state theory (VTST)[73] calculations were performed to estimate the rate constants of internal conversion (k_{int}) and the desorption of CO (k_d) from the concerned stable intermediates (Tables S2–S6). For the reaction of $B_6O_n^+$ (n = 0–3) with CO_2, Tables S2–S5 show that rate constants k_{int} ($\geq 10^8$) and k_d ($\geq 10^8$) at each step of the reaction are about 1000 times bigger than the rate constant of collision between the $B_6O_n^+$ clusters and the He gas in the LIT reactor (2.05×10^5 s^{-1}). Thus, CO ligands in the CO-desorption states of the corresponding reaction pathways are easily released into the gas phase, in excellent agreement with experimental findings that no corresponding CO_2 adsorption products such as $B_6CO_2^+$, $B_6OCO_2^+$, $B_6O_2CO_2^+$, and $B_6O_3CO_2^+$ were observed in the mass spectrometry data (Figs. 1 and S2). However, for the reactions of $B_6O_n^+$ + CO_2 (n = 4–6) (Figs. 2, S16, and S17), the k_{int} values for **IM49** → **TS42** in the $B_6O_4^+/CO_2$ system, **IM61** → **TS53** in $B_6O_5^+/CO_2$, and **IM9** → **TS7** in $B_6O_6^+/CO_2$ (Tables S6–S8) are either slightly larger or smaller than the collision rate constant (2.05×10^5 s^{-1}). This suggests that **IM49, IM61, and IM9** may be collisionally stabilized before overcoming the corresponding barriers, leading to the experimentally observed weak $B_6O_nCO_2^+$ (n = 4–6) signals in Figs. 1 and S2. Furthermore, **7B** can adsorb CO_2 to form a stable encounter complex, **IM72**, with a binding energy of 1.20 eV. However, the subsequent activation of CO_2 requires overcoming a positive barrier of 0.14 eV (Fig. S18). Therefore, **IM72** is likely to correspond to the experimentally observed $B_6O_7CO_2^+$ species.

IV. DISCUSSION

A. AdNDP bonding pattern analyses

To better comprehend the reaction pathways obtained in Fig. 2, as demonstrations, we performed detailed AdNDP bonding pattern analyses shown in Fig. 4 on the most concerned reactants, intermediates, and products of the reaction $B_6^+ + CO_2 \rightarrow B_6O^+ + CO$ shown in Fig. 2(a). As expected, a free linear O=C=O molecule contains two 2c-2e C–O σ bonds and two 2c-2e C–O π bonds. The isolated perfect planar C_{2h} B_6^+ (**iso1**) possesses six 2c-2e B–B periphery σ bonds, one fully delocalized 6c-2e σ bond, one fully delocalized 6c-2e π bond, and one singly occupied 6c-1e σ bond (SOMO) [Fig. 4(a)]. Interestingly, in the CO_2-adsorption state C_s $[B_6–O–C≡O]^+$ (**IM1**), an extra 2c-2e B ← O–C≡O σ-donation bond is formed between the most protruding di-coordinate vertex B atom as the first active site in B_6^+ and the :O–C≡O σ-ligand, meanwhile, the 2c-2e O–C π bond on the left side of O=C=O ligand is activated in the first reaction step to the form a C≡O triple bond in the –C≡O terminal at the right end, which contains one C–O σ-bond and two C–O π-bonds. The first B active site, therefore, plays a major role in activating one π-bond in O=C=O to form the first CO_2-adsorption state $[B_6–O–C≡O]^+$ (**IM1**). The six 2c-2e B–B periphery σ-bonds, one delocalized 6c-2e σ bond, and one totally delocalized 6c-2e π bond over the B_6^+ (**iso 1**) framework are well-inherited in **IM1**. However, the CO_2-adsorption state **IM1** possesses an unexpected singly occupied 6c-1e π-bond as the SOMO of the system. Meanwhile, both the CO-desorption state $[OB_6–CO]^+$ (**IM3**) and final product B_6O^+ (**P1**) formed by releasing a CO molecule from the second active B site possess one 7c-2e σ bond, one 7c-2e π bond, and one singly

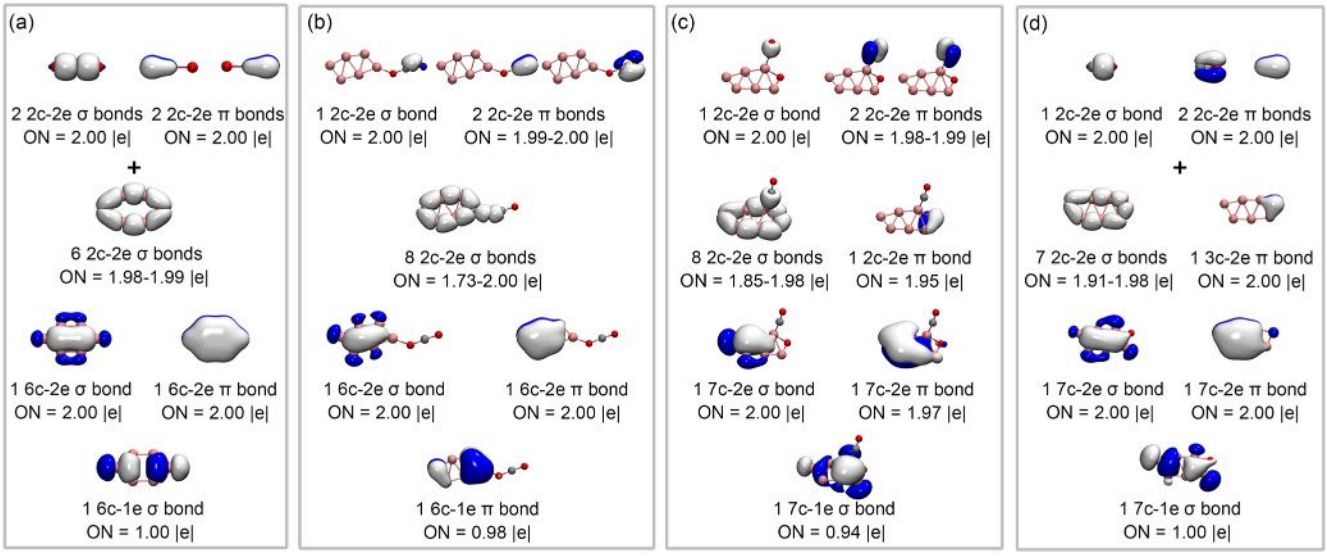

FIG. 4. AdNDP bonding patterns of (a) $CO_2 + B_6^+$ (**iso 1**), (b) $[B_6–O–C≡O]^+$ (**IM1**), (c) $[OB_6–CO]^+$ (**IM3**), and (d) $CO + B_6O^+$ (**P1**), with the lone pairs on O atoms omitted and occupation numbers (ON) indicated.

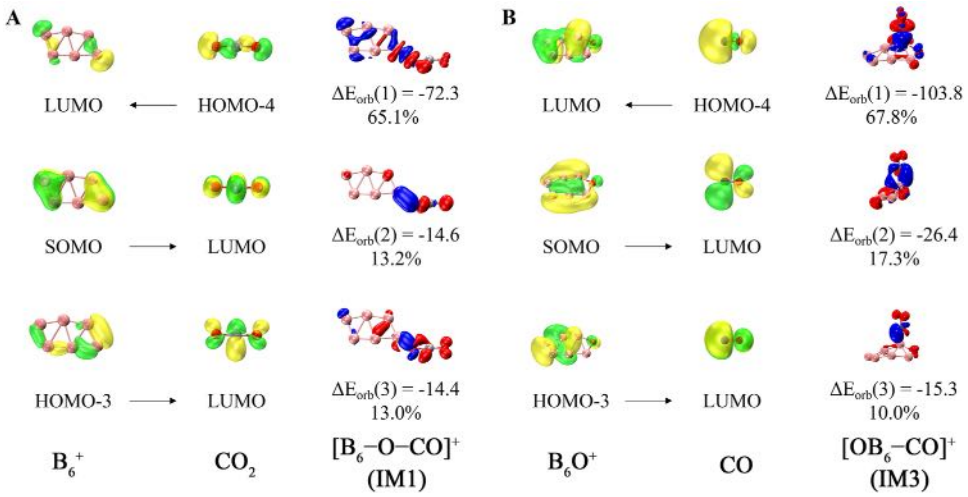

FIG. 5. Plots of the deformation densities $\Delta\rho$ and shapes of the most important interacting orbitals of the pairwise orbital interactions (A) between B_6^+(**iso 1**) and :O–C≡O in $[B_6–O–C≡O]^+$ (**IM1**) and (B) between B_6O^+ and CO in $[OB_6–CO]^+$ (**IM3**), with the orbital interaction energies ΔE_{orb} in kcal mol^{-1} and their percentage contributions to the overall orbital interactions indicated. The color code of the charge flow is red → blue.

occupied 7c-1e σ-SOMO, indicating that a σ → π→ σ transition occurs to the SOMOs of the system via the first CO_2-adsorption state $[B_6–O–C≡O]^+$ (**IM1**). The existence of such a σ → π → σ orbital transition favors the formation of one effective σ-donation bond and two weak π-back-donations between the B_6^+ coordination center and :O–C≡O σ-ligand in **IM1**, which will be discussed in detail next. Similar bonding pattern evolutions exist in other reaction pathways.

B. EDA-NOCV coordination interaction analyses

Detailed EDA-NOCV analyses of the CO_2-adsorption state $[B_6–O–C≡O]^+$(**IM1**) using B_6^+ (**iso 1**) and CO_2 as interaction fragments shown in Fig. 5(A) and Table S9 indicate that the HOMO-4 orbital of O=C=O donates a σ-lone pair on O to the LUMO orbital of B_6^+ to form an effective σ-donation coordination bond, accounting for 65.1% of the overall orbital interaction energy (ΔE_{orb}). The SOMO and HOMO-3 of B_6^+ donate partial electrons back to the two degenerate anti-bonding orbitals (LUMOs) of O=C=O, forming two weak π-backdonations perpendicular to each other, which contribute 13.2% and 13.0% to the overall orbital interaction energy ΔE_{orb}, respectively. The effective σ-donation interaction is well-reflected in the 2c-2e B ← O–C≡O σ-donation bond in Fig. 4(b) in the AdNDP bonding pattern of the $[B_6–O–C≡O]^+$ (**IM1**). Such a σ + 2π coordination bonding pattern shows that the first di-coordinate periphery B atom as an active site exhibits transition-metal-like behaviors in the activation of CO_2. EDA-NOCV analyses in Fig. 5(B) and Table S10 unveil a similar σ + 2π coordination bonding pattern in the CO-desorption state $[OB_6–CO]^+$ (**IM3**), which possesses one effective σ-donation (67.8%) from the HOMO-4 of CO to the LUMO of B_6O^+, one weak π-backdonation (17.3%) from the SOMO of B_6O^+ to the LUMO of CO, and another weak π-backdonation (10.0%) from the HOMO-3 of B_6O^+ to LUMO of CO, indicating that the second active di-coordinate B atom also behaves like a transition metal atom in the CO-desorption process.

V. CONCLUSIONS

Extensive joint gas-phase mass spectroscopy and first-principles theory investigations performed in this work indicate that a mass-selected B_6^+ monocation can activate and convert up to seven CO_2 to CO molecules consecutively at room temperature via barrier-free mechanisms, presenting the maximum number of CO_2 molecules that an isolated nanocluster can activate in experiments reported to date. Two periphery B atoms in $B_6O_n^+$ (n = 0–6) are found to serve as active sites in two consecutive steps to activate one π-bond in O=C=O to form the O≡C–O-adsorption states and to release a CO molecule from the CO-desorption states to form the final products $B_6O_{n+1}^+$, respectively, unveiling the unique role of boron as an honorary transition metal in CO_2 activation and conversion. These findings provide important insights into designing novel boron-containing nanocatalysts and nanomaterials to activate CO_2 to release CO or to form other high value-added chemicals. Boron activation and catalysis are expected to have unique and important applications in chemistry and materials science at nanoscales.

SUPPLEMENTARY MATERIAL

The supplementary material includes additional TOF mass spectra and reaction rates for $B_m^+ + CO_2$ (m = 5–15), low-lying isomers of $B_6O_n^+$ (n = 0–7), potential energy profiles for $B_6O_n^+ + CO_2$ (n = 0–7), BOMD simulations of the most stable $B_6O_n^+$ (n = 1–7), ESP and NBO analyses of $B_6O_n^+$ (n = 0–7), and EDA-NOCV analyses for **IM1** and **IM3**.

ACKNOWLEDGMENTS

This work was supported by the National Natural Science Foundation of China (Grant Nos. 22003034, 92461303, and 22373061).

AUTHOR DECLARATIONS

Conflict of Interest

The authors have no conflicts to disclose.

Author Contributions

Q. Chen and R.-N. Yuan contributed equally to this work.

Q.C., S.-G.H., and S.-D.L. conceived the concepts. Q.C. supervised the experimental work, and Q.C. and S.-D.L. supervised the theoretical work. R.-N.Y. and H.N. performed the experiments. R.-N.Y., Q.-W.Z., R.W., Z.-H.W., and H.-G.L. carried out the theoretical calculations. Q.C., R.-N.Y., and S.-D.L. co-wrote the article. All authors contributed to the discussion and commented on the manuscript.

Qiang Chen: Conceptualization (lead); Data curation (equal); Formal analysis (equal); Funding acquisition (lead); Investigation (equal); Methodology (equal); Project administration (equal); Resources (equal); Supervision (equal); Validation (equal); Visualization (equal); Writing – original draft (equal); Writing – review & editing (equal). **Rui-Nan Yuan**: Data curation (equal); Formal analysis (equal); Investigation (equal); Validation (equal); Visualization (equal); Writing – original draft (equal). **Qin-Wei Zhang**: Formal analysis (equal); Investigation (equal). **Hong Niu**: Formal analysis (equal); Investigation (equal). **Rui Wei**: Formal analysis (equal); Investigation (equal). **Zhi-Hong Wei**: Formal analysis (equal); Visualization (equal). **Hai-Gang Lu**: Investigation (equal). **Sheng-Gui He**: Conceptualization (equal); Formal analysis (equal); Methodology (equal). **Si-Dian Li**: Conceptualization (equal); Data curation (equal); Formal analysis (equal); Funding acquisition (lead); Investigation (equal); Methodology (equal); Project administration (equal); Resources (lead); Supervision (equal); Writing – original draft (equal); Writing – review & editing (equal).

DATA AVAILABILITY

The data that support the findings of this study are available within the article and its supplementary material.

REFERENCES

[1] P. Gao, S. Li, X. Bu, S. Dang, Z. Liu, H. Wang, L. Zhong, M. Qiu, C. Yang, J. Cai, W. Wei, and Y. Sun, Nat. Chem. **9**, 1019 (2017).
[2] R. P. Ye, J. Ding, W. Gong, M. D. Argyle, Q. Zhong, Y. Wang, C. K. Russell, Z. Xu, A. G. Russell, Q. Li, M. Fan, and Y. G. Yao, Nat. Commun. **10**, 5698 (2019).
[3] G. Wang, J. Chen, Y. Ding, P. Cai, L. Yi, Y. Li, C. Tu, Y. Hou, Z. Wen, and L. Dai, Chem. Soc. Rev. **50**, 4993 (2021).
[4] M. He, Y. Sun, and B. Han, Angew. Chem., Int. Ed. **61**, e202112835 (2022).
[5] Q. Liu, L. Wu, R. Jackstell, and M. Beller, Nat. Commun. **6**, 5933 (2015).
[6] Y. Y. Birdja, E. Pérez-Gallent, M. C. Figueiredo, A. J. Göttle, F. Calle-Vallejo, and M. T. M. Koper, Nat. Energy **4**, 732 (2019).
[7] M. Ghoussoub, M. Xia, P. N. Duchesne, D. Segal, and G. Ozin, Energy Environ. Sci. **12**, 1122 (2019).
[8] E. E. Barton, D. M. Rampulla, and A. B. Bocarsly, J. Am. Chem. Soc. **130**, 6342 (2008).
[9] H. Schwarz, Coord. Chem. Rev. **334**, 112 (2017).
[10] X. Wang, H. Shi, J. H. Kwak, and J. Szanyi, ACS Catal. **5**, 6337 (2015).
[11] X. Su, X. F. Yang, Y. Huang, B. Liu, and T. Zhang, Acc. Chem. Res. **52**, 656 (2019).
[12] H. Braunschweig, R. D. Dewhurst, F. Hupp, M. Nutz, K. Radacki, C. W. Tate, A. Vargas, and Q. Ye, Nature **522**, 327 (2015).
[13] W. J. Tian, W. J. Chen, M. Yan, R. Li, Z. H. Wei, T. T. Chen, Q. Chen, H. J. Zhai, S. D. Li, and L. S. Wang, Chem. Sci. **12**, 8157 (2021).
[14] R. N. Yuan, J. J. Chen, Q. Chen, Q. W. Zhang, H. Niu, R. Wei, Z. H. Wei, X. N. Li, and S. D. Li, J. Am. Chem. Soc. **146**, 31464 (2024).
[15] R. N. Yuan, Q. Chen, H. Niu, C. Y. Gao, X. N. Zhao, Y. B. Wu, S. G. He, and S. D. Li, Phys. Chem. Chem. Phys. **27**, 7279 (2025).
[16] H. Niu, Q. Chen, R. N. Yuan, Q. W. Zhang, and S. D. Li, Phys. Chem. Chem. Phys. **27**, 17922 (2025).
[17] A. N. Alexandrova, A. I. Boldyrev, H. J. Zhai, and L. S. Wang, Coord. Chem. Rev. **250**, 2811 (2006).
[18] A. P. Sergeeva, I. A. Popov, Z. A. Piazza, W.-L. Li, C. Romanescu, L. S. Wang, and A. I. Boldyrev, Acc. Chem. Res. **47**, 1349 (2014).
[19] T. Jian, X. Chen, S. D. Li, A. I. Boldyrev, J. Li, and L. S. Wang, Chem. Soc. Rev. **48**, 3550 (2019).
[20] H. Bai, T. T. Chen, Q. Chen, X. Y. Zhao, Y. Y. Zhang, W. J. Chen, W. L. Li, L. F. Cheung, B. Bai, J. Cavanagh, W. Huang, S. D. Li, J. Li, and L. S. Wang, Nanoscale **11**, 23286 (2019).
[21] Y. J. Wang, Y. F. Zhao, W. L. Li, T. Jian, Q. Chen, X. R. You, T. Ou, X. Y. Zhao, H. J. Zhai, S. D. Li, J. Li, and L. S. Wang, J. Chem. Phys. **144**, 064307 (2016).
[22] H. J. Zhai, Y. F. Zhao, W. L. Li, Q. Chen, H. Bai, H. S. Hu, Z. A. Piazza, W. J. Tian, H. G. Lu, Y. B. Wu, Y. W. Mu, G. F. Wei, Z. P. Liu, J. Li, S. D. Li, and L. S. Wang, Nat. Chem. **6**, 727 (2014).
[23] Q. Chen, W. L. Li, Y. F. Zhao, S. Y. Zhang, H. S. Hu, H. Bai, H. R. Li, W. J. Tian, H. G. Lu, H. J. Zhai, S. D. Li, J. Li, and L. S. Wang, ACS Nano **9**, 754 (2015).
[24] W. J. Chen, Y. Y. Ma, T. T. Chen, M. Z. Ao, D. F. Yuan, Q. Chen, X. X. Tian, Y. W. Mu, S. D. Li, and L. S. Wang, Nanoscale **13**, 3868 (2021).
[25] Q. Chen, H. W. Choi, G. F. Wei, D. Kahraman, R. N. Yuan, Q. W. Zhang, Q. Q. Yan, X. N. Zhao, C. Y. Gao, Y. Y. Ma, R. Wei, Y. Gui, Z. P. Liu, S. D. Li, and L. S. Wang, Proc. Natl. Acad. Sci. U. S. A. **122**, e2510702122 (2025).
[26] E. Oger, N. R. M. Crawford, R. Kelting, P. Weis, M. M. Kappes, and R. Ahlrichs, Angew. Chem., Int. Ed. **46**, 8503 (2007).
[27] M. A. Légaré, G. Bélanger-Chabot, R. D. Dewhurst, E. Welz, I. Krummenacher, B. Engels, and H. Braunschweig, Science **359**, 896 (2018).
[28] M. A. Légaré, M. Rang, G. Bélanger-Chabot, J. I. Schweizer, I. Krummenacher, R. Bertermann, M. Arrowsmith, M. C. Holthausen, and H. Braunschweig, Science **363**, 1329 (2019).
[29] K. T. Smith, S. Berritt, M. González-Moreiras, S. Ahn, M. R. Smith, M. H. Baik, and D. J. Mindiola, Science **351**, 1424 (2016).
[30] H. Braunschweig, T. Dellermann, R. D. Dewhurst, W. C. Ewing, K. Hammond, J. O. C. Jimenez-Halla, T. Kramer, I. Krummenacher, J. Mies, A. K. Phukan, and A. Vargas, Nat. Chem. **5**, 1025 (2013).
[31] A. K. Cook, S. D. Schimler, A. J. Matzger, and M. S. Sanford, Science **351**, 1421 (2016).
[32] G. Liu, X. Meng, H. Zhang, G. Zhao, H. Pang, T. Wang, P. Li, T. Kako, and J. Ye, Angew. Chem., Int. Ed. **56**, 5570 (2017).
[33] M.-A. Légaré, M. A. Courtemanche, É. Rochette, and F. G. Fontaine, Science **349**, 513 (2015).
[34] S. A. Ruatta, P. A. Hintz, and S. L. Anderson, J. Chem. Phys. **94**, 2833 (1991).
[35] Q. Chen, Y. X. Zhao, L. X. Jiang, J. J. Chen, and S. G. He, Angew. Chem., Int. Ed. **57**, 14134 (2018).
[36] H. Y. Zhou, M. Wang, Y. Q. Ding, and J. B. Ma, Dalton Trans. **49**, 14081 (2020).
[37] Z. Y. Chen, M. Wang, Y. Q. Ding, and J. B. Ma, J. Phys. Chem. A **127**, 3082 (2023).
[38] Y. H. Zhang and J. B. Ma, J. Phys. Chem. A **128**, 2323 (2024).
[39] X. Y. He, Y. Z. Liu, J. J. Chen, X. Lan, X. N. Li, and S. G. He, J. Phys. Chem. Lett. **14**, 6948 (2023).
[40] R. A. J. O'Hair, Chem. Commun. **14**, 1469 (2006).
[41] L. D. Socaciu, J. Hagen, U. Heiz, T. M. Bernhardt, T. Leisner, and L. Wöste, Chem. Phys. Lett. **340**, 282 (2001).
[42] X. N. Wu, B. Xu, J. H. Meng, and S. G. He, Int. J. Mass Spectrom. **310**, 57 (2012).
[43] Z. Yuan, Z. Y. Li, Z. X. Zhou, Q. Y. Liu, Y. X. Zhao, and S. G. He, J. Phys. Chem. C **118**, 14967 (2014).
[44] C. Lee, W. Yang, and R. G. Parr, Phys. Rev. B **37**, 785 (1988).
[45] A. D. Becke, Phys. Rev. A **38**, 3098 (1988).
[46] A. D. Becke, J. Chem. Phys. **98**, 5648 (1993).
[47] A. Schäfer, C. Huber, and R. Ahlrichs, J. Chem. Phys. **100**, 5829 (1994).
[48] R. A. Kendall, T. H. Dunning, and R. J. Harrison, J. Chem. Phys. **96**, 6796 (1992).
[49] G. D. Purvis and R. J. Bartlett, J. Chem. Phys. **76**, 1910 (1982).

[50]G. E. Scuseria and H. F. Schaefer, J. Chem. Phys. **90**, 3700 (1989).
[51]G. E. Scuseria, C. L. Janssen, and H. F. Schaefer, J. Chem. Phys. **89**, 7382 (1988).
[52]P. Celani and H. J. Werner, J. Chem. Phys. **112**, 5546 (2000).
[53]K. Andersson, P.-Å. Malmqvist, and B. O. Roos, J. Chem. Phys. **96**, 1218 (1992).
[54]Y. Zhao, X. Chen, and J. Li, Nano Res. **10**, 3407 (2017).
[55]X. Chen, Y.-F. Zhao, L.-S. Wang, and J. Li, Comput. Theor. Chem. **1107**, 57 (2017).
[56]C. Gonzalez and H. B. Schlegel, J. Chem. Phys. **90**, 2154 (1989).
[57]C. Gonzalez and H. B. Schlegel, J. Phys. Chem. **94**, 5523 (1990).
[58]M. J. Frisch, G. W. Trucks, H. B. Schlegel, G. E. Scuseria, M. A. Robb, J. R. Cheeseman, G. Scalmani, V. Barone, G. A. Petersson, H. Nakatsuji, X. Li, M. Caricato, A. V. Marenich, J. Bloino, B. G. Janesko, R. Gomperts, B. Mennucci, H. P. Hratchian, J. V. Ortiz, A. F. Izmaylov, J. L. Sonnenberg, D. Williams-Young, F. Ding, F. Lipparini, F. Egidi, J. Goings, B. Peng, A. Petrone, T. Henderson, D. Ranasinghe, V. G. Zakrzewski, J. Gao, N. Rega, G. Zheng, W. Liang, M. Hada, M. Ehara, K. Toyota, R. Fukuda, J. Hasegawa, M. Ishida, T. Nakajima, Y. Honda, O. Kitao, H. Nakai, T. Vreven, K. Throssell, J. A. Montgomery, Jr., J. E. Peralta, F. Ogliaro, M. J. Bearpark, J. J. Heyd, E. N. Brothers, K. N. Kudin, V. N. Staroverov, T. A. Keith, R. Kobayashi, J. Normand, K. Raghavachari, A. P. Rendell, J. C. Burant, S. S. Iyengar, J. Tomasi, M. Cossi, J. M. Millam, M. Klene, C. Adamo, R. Cammi, J. W. Ochterski, R. L. Martin, K. Morokuma, O. Farkas, J. B. Foresman, and D. J. Fox, *Gaussian 16, Revision A.03*, Gaussian, Inc., Wallingford, CT, 2016.
[59]H. J. Werner, P. J. Knowles, G. Knizia, F. R. Manby, M. Schutz, P. Celani, T. Korona, R. Lindh, A. Mitrushenkov, G. Rauhut, K. R. Shamasundar, T. B. Adler, R. D. Amos, A. Bernhardsson, A. Berning, D. L. Cooper, M. J. O. Deegan, A. J. Dobbyn, F. Eckert, E. Goll, C. Hampel, A. Hesselmann, G. Hetzer, T. Hrenar, G. Jansen, C. Koppl, Y. Liu, A. W. Lloyd, R. A. Mata, A. J. May, S. J. McNicholas, W. Meyer, M. E. Mura, A. Nicklass, D. P. O'Neill, P. Palmieri, D. Peng, K. Pfluger, R. Pitzer, M. Reiher, T. Shiozaki, H. Stoll, A. J. Stone, R. Tarroni, T. Thorsteinsson, and M. Wang, MOLPRO *2012.1*, University College Cardiff Consultants Limited, Cardiff, 2012.
[60]E. D. Glendening, J. K. Badenhoop, A. E. Reed, J. E. Carpenter, J. A. Bohmann, C. M. Morales, C. R. Landis, and F. Weinhold, *NBO 6.0*, Theoretical Chemistry Institute, University of Wisconsin, Madison, WI, 2013, http://nbo6.chem.wisc.edu/.
[61]S. Goedecker, M. Teter, and J. Hutter, Phys. Rev. B **54**, 1703 (1996).
[62]W. L. Li, K. Chen, E. Rossomme, M. Head-Gordon, and T. Head-Gordon, J. Phys. Chem. Lett. **12**, 10304 (2021).
[63]J. VandeVondele, M. Krack, F. Mohamed, M. Parrinello, T. Chassaing, and J. Hutter, Comput. Phys. Commun. **167**, 103 (2005).
[64]N. V. Tkachenko and A. I. Boldyrev, Phys. Chem. Chem. Phys. **21**, 9590 (2019).
[65]T. Ziegler and A. Rauk, Theor. Chim. Acta **46**, 1 (1977).
[66]M. P. Mitoraj, A. Michalak, and T. Ziegler, J. Chem. Theory Comput. **5**, 962 (2009).
[67]M. Mitoraj and A. Michalak, Organometallics **26**, 6576 (2007).
[68]G. te Velde, F. M. Bickelhaupt, E. J. Baerends, C. Fonseca Guerra, S. J. A. van Gisbergen, J. G. Snijders, and T. Ziegler, J. Comput. Chem. **22**, 931 (2001).
[69]J. Li, C. Geng, T. Weiske, and H. Schwarz, Angew. Chem., Int. Ed. **59**, 12308 (2020).
[70]T. B. Tai, N. M. Tam, and M. T. Nguyen, Theor. Chem. Acc. **131**, 1241 (2012).
[71]R. Shinde and A. Shukla, Eur. Phys. J. D **67**, 98 (2013).
[72]E. M. I. Moreira, B. G. A. Brito, G.-Q. Hai, and L. Cândido, Phys. Chem. Chem. Phys. **24**, 3119 (2022).
[73]J. I. Steinfeld, J. S. Francisco, and W. L. Hase, *Chemical Kinetics and Dynamics* (Prentice-Hall, Upper Saddle River, NJ, 1999), pp. 231–313.